

Time-Domain Measurement of the Frequency-Dependent Delay of Broadband Antennas

Jason D. McKinney, *Member, IEEE*, Dimitrios Peroulis, *Member, IEEE*, and Andrew M. Weiner, *Fellow, IEEE*

Abstract—We present a new time-domain technique for direct measurement of the frequency-dependent delay of broadband antenna structures. By utilizing a series of fixed-bandwidth, variable center frequency waveforms synthesized in a photonics-based electromagnetic pulse shaper, we perform high time resolution (~ 54 ps over ~ 10 ns) measurements of several broadband antenna structures. Our results show excellent agreement with the delay extracted via time-domain impulse response measurements, however, compared to conventional impulse response measurements, our method ensures a higher signal-to-noise ratio because it relies on several relatively narrowband measurements as opposed to a single broadband measurement. In addition, the delay uncertainty in our technique (~ 54 ps) is significantly below that of impulse response measurements (~ 300 ps) where numerical differentiation of noisy data leads to substantial errors. Our technique is well suited as a diagnostic tool for future variable-frequency fixed-bandwidth systems.

Index Terms—Broadband antennas, radio-frequency (RF) photonics, time-domain techniques, ultrawideband (UWB).

I. INTRODUCTION

WITH substantial interest in ultrawideband (UWB) systems for applications such as ground-penetrating radar [1] and wireless communication [1], [2], it is extremely important to characterize the effects of broadband antennas on large fractional-bandwidth signals. In particular, the ability to measure the frequency-dependent delay (dispersion) of a broadband antenna structure is of key importance. With knowledge of this nonuniform radio-frequency (RF) spectral phase response, one has the potential to compensate for the time-domain broadening and distortion this response imparts to UWB signals.

Frequency-domain measurements of the RF spectral phase properties of a system (antenna) are well established in the laboratory [4]; here, we focus on time-domain antenna measurements that are suitable for either laboratory or system (*in situ*) environments. The impulse response is the most commonly accepted time-domain method of obtaining the frequency response of a linear system (e.g., an antenna link). Provided one excites the link with a sufficiently short-duration (broad bandwidth) signal, one may obtain the link frequency response

(amplitude and phase, or delay) via a fast-Fourier transform (FFT) of the time-domain data. One may alternatively extract the frequency-dependent delay properties of the link (or, more appropriately, the antennas utilized in the link) directly. Various techniques to accomplish such a direct measurement are known and practiced in the ultrafast optics community. Of particular relevance is a technique that employs tunable-frequency burst optical signals to extract the group delay of a material placed within an interferometer [5]. To our knowledge, however, such direct time-domain frequency-dependent delay measurements have not previously been applied in the UWB RF domain.

In this work, we utilize a photonics-based electromagnetic pulse shaper [6], [7] to perform direct frequency-dependent delay measurements for several broadband antenna structures. By characterizing wireless links consisting of a pair of identical antennas, we demonstrate that we may use the delay extracted from these measurements to predict the behavior of asymmetric antenna links (those constructed using two different antenna structures). Our technique demonstrates excellent sensitivity to frequency-dependent delay variations and may be applied as an alternative to either time-domain impulse response or frequency-domain measurements to characterize the dispersion of broadband antenna structures. The instantaneous RF bandwidth required by our technique is ~ 16 -times lower than that of an equivalent impulse response measurement. Since our signal generation apparatus is peak power limited, this decrease in bandwidth leads to an increased signal-to-noise ratio (SNR) in our technique as compared to impulse response measurements. Furthermore, our technique is applicable over a very broad frequency range and provides a novel diagnostic tool for future systems.

We note that vector network analyzers (VNAs) are widely employed to perform measurements of the frequency-dependent delay of microwave systems and, of particular relevance to this work, broadband antennas. While outside the scope of the effort presented here, a comparison of the delay obtained via conventional VNA measurements to that obtained with our technique presents an interesting area for future study. Several points are worth noting, however, in particular VNA measurements (as with impulse response measurements) measure the RF spectral phase and the frequency-dependent delay is obtained via a derivative. This operation has the potential to negate the gain in SNR obtained by the narrow-bandwidth excitation in swept-frequency measurements. Our technique, on the other hand, measures the frequency-dependent delay directly and does not suffer from the additional noise penalty incurred by differentiating the RF spectral phase. From a practical perspective, for those performing research in “impulsive” UWB systems, our electromagnetic pulse shaping apparatus may be used to both measure and

Manuscript received January 15, 2007; revised August 30, 2007. This work was supported by the U.S. Army Research Office under Contract DAAD19-03-1-0275.

J. D. McKinney was with the School of Electrical and Computer Engineering, Purdue University, West Lafayette, IN 47907–2035 USA. He is now with the Microwave Photonics Section, Optical Sciences Division, U.S. Naval Research Laboratory, Washington, DC 20375-5337 USA (e-mail: jason.mckinney@nrl.navy.mil).

D. Peroulis and A. M. Weiner are with the School of Electrical and Computer Engineering, Purdue University, West Lafayette, IN 47907–2035 USA.

Digital Object Identifier 10.1109/TAP.2007.913079

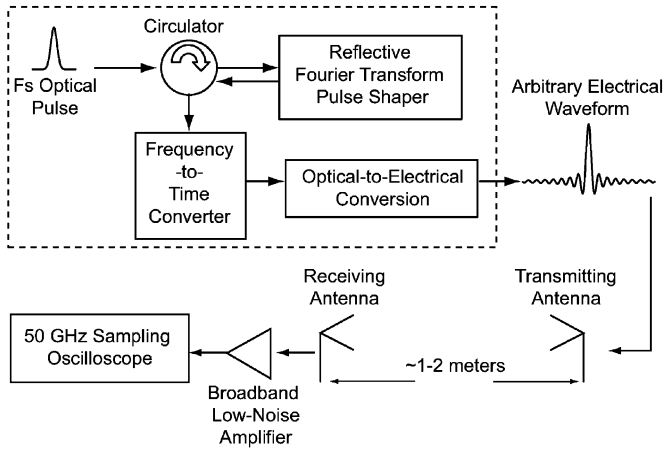


Fig. 1. Schematic representation antenna measurement apparatus that employs our time-domain electromagnetic pulse shaper (enclosed by the dashed line), which provides arbitrary RF waveforms with up to ~ 3 ns duration and 11 GHz bandwidth. These waveforms excite one of several broadband antennas; a subsequent broadband antenna functions as a receiver. The received waveforms are amplified and measured via a 50 GHz sampling oscilloscope.

compensate for phase distortions in these systems. Our technique may also be extended to measurements where a VNA may not be employed directly, such as those involving nonlinear microwave systems (e.g., amplifiers operating in compression) where the system output is dependent on the particular excitation waveform.

Our paper is organized as follows. In Section II, we review the salient aspects of our photonics-based electromagnetic pulse shaper. Section III reviews the concept of frequency-dependent delay and details our time-domain measurement methodology. In Section IV, we provide direct frequency-dependent delay measurements for both low-dispersion and highly-dispersive antenna links (constructed from several types of broadband antennas) and introduce the use of spectrograms to visualize and analyze our delay data. In this section we also illustrate the excellent agreement between the delay measured in our technique to that obtained via the link impulse response. At the end of this Section, we illustrate that our delay measurements enable us to quite accurately predict the behavior of wireless links constructed using different antenna structures. In Section V, we conclude.

II. PHOTONICS-BASED ELECTROMAGNETIC PULSE SHAPING AND EXPERIMENTAL APPARATUS

Our experimental apparatus utilizes arbitrary RF waveforms synthesized with a photonics-based electromagnetic pulse shaper, shown schematically in Fig. 1 (enclosed by the dashed line). The waveforms from our electromagnetic pulse shaper then form the input excitation to a wireless link consisting of a pair of broadband antennas. Functionally, the electromagnetic pulse shaper utilizes established optical pulse shaping technology to shape the power spectrum of an input short pulse. This pulse is subsequently dispersed in a length of optical fiber. The chromatic dispersion of the optical fiber uniquely maps optical frequency to time which results in a time-domain waveform (current) from the photodiode with a temporal shape

determined by that of the tailored optical power spectrum. For a detailed discussion, please consult [6] and [7]. In our apparatus' current configuration, the waveform time aperture is approximately 3 ns and the finest temporal feature is ~ 45 ps; the latter yields an RF bandwidth of 11 GHz. This electromagnetic pulse shaping technique provides unprecedented waveform agility and enables a variety of excitation waveforms for our antenna system, which range from broadband sinusoids (constant frequency as well as frequency-stepped) [6] to highly-structured UWB impulses [7]. We note that our technique allows direct-specification of the output electrical waveform; others have demonstrated a similar technique [8] which iteratively solves for sinusoidal and frequency-modulated waveforms.

Two aspects of the arbitrary waveforms generated in our electromagnetic pulse shaper are particularly pertinent to the measurements presented here [7]. First, our apparatus maps one optical pulse to one electrical waveform. After the optical pulse is dispersed in the fixed-length fiber stretcher the optical (electrical) waveform duration is also fixed; the combination of a fixed optical energy and fixed waveform duration enforces a peak-power limit on our waveforms. This limitation is not unique to our apparatus and is in fact a primary motivation for measuring the frequency-dependent delay (in contrast to the impulse response). For bandwidth-limited duration signals constrained to a fixed peak-power, a narrower signal bandwidth yields a larger waveform energy. It is advantageous from a measurement perspective, then, to utilize narrowband waveforms at different center frequencies as opposed to a broadband impulse.

The second important aspect is that our waveforms are required to be positive-definite as determined by the mapping of optical intensity to electrical voltage (current). Since our waveforms are all of limited duration, this constraint means that waveforms from our apparatus will necessarily possess a baseband spectral component determined by the waveform envelope. All waveforms—irrespective of the particular modulation frequency—will possess the same baseband component provided the envelope shape is fixed. Therefore, the waveform duration must be chosen to avoid unwanted low-frequency content in the radiated (received) waveform. We further elaborate on these aspects of our waveforms, relative to our measurement technique, in the following sections.

III. FREQUENCY-DEPENDENT DELAY AND VARIABLE-FREQUENCY FIXED BANDWIDTH WAVEFORMS

The measurement technique presented in this work provides a direct measurement of the frequency-dependent delay imparted by one (or both) of the broadband antennas in a wireless link. We note that, in the time-domain, the most common method for extracting the RF spectral phase response of a broadband antenna (as well as the frequency-dependent delay) is via the antenna impulse response—this has been demonstrated by others experimentally [9] and predicted numerically [10] for a variety of broadband antennas. Here, we demonstrate our technique yields the same information as the link impulse response, while offering the advantage of increased transmitted and received waveform energy in a peak-power limited system.

Conceptually, the technique presented here is analogous to frequency-domain measurements performed with a vector network analyzer. In frequency-domain measurements, the single-tone received voltage signal ($|V_{\text{sig}}(\omega)| \exp[j\phi_{\text{sig}}(\omega)]$) is compared to that of the source oscillator ($|V_{\text{in}}(\omega)| \exp[j\phi_{\text{in}}(\omega)]$) as it is swept over a user-defined frequency range to yield the system (antenna or antenna link) frequency response

$$|H_l(\omega)| \exp[j\phi_l(\omega)] = \frac{|V_{\text{sig}}(\omega)|}{|V_{\text{in}}(\omega)|} \exp\{j[\phi_{\text{sig}}(\omega) - \phi_{\text{in}}(\omega)]\}. \quad (1)$$

The frequency-dependent delay of the system is then related to the measured RF spectral phase through the relation

$$\tau_l(\omega) = -\frac{d\phi_l(\omega)}{d\omega} \quad (2)$$

where a $+j\omega t$ phasor time-dependence is assumed. To perform a time-domain measurement of the frequency-dependent delay, we utilize a series of fixed-bandwidth Gaussian pulses amplitude-modulated by sinusoids at several discrete center frequencies as our transmit waveforms. These waveforms are synthesized in our electromagnetic pulse shaper and are of the form

$$v_{\text{in}}(t) = 1/2[1 + \cos(2\pi f_o t)] \exp(-t^2/t_o^2). \quad (3)$$

The voltage waveform fullwidth at half-maximum (FWHM) duration is chosen to be $\Delta t \approx 1.14$ ns (Gaussian envelope with $t_o = 0.684$ ns) which gives a FWHM spectral amplitude (voltage) bandwidth of $\Delta f \approx 775$ MHz. The frequency-dependent delay of the antenna link is then determined by measuring the difference in pulse arrival time as a function of the pulse center frequency. We discuss the utility of this technique for characterizing several broadband antenna geometries in the following section. As mentioned earlier, these waveforms are positive definite which is an artifact of our electromagnetic pulse shaper; however, the bandwidth of the baseband component is approximately 380 MHz which falls below the cutoff frequency of the majority of the antennas discussed here. This component, therefore, does not affect the frequency-dependent delay measurements presented here.

IV. FREQUENCY-DEPENDENT DELAY MEASUREMENTS

In this work, we construct a time-domain antenna link which comprises a pair of broadband antennas. The output of the receiving antenna is amplified with a low-noise amplifier (gain of ~ 30 dB from 0.1–18 GHz) and measured with a 50 GHz sampling oscilloscope as illustrated in Fig. 1. We have chosen to focus on three antenna geometries in this work: commercial Archimedean spiral antennas (NURAD 96C4100, 1–18 GHz) [11] which are known to be strongly dispersive; commercial ridged-horn antennas (Dorado International GH1-12N, 1–12 GHz) that exhibit strong dispersion at low frequencies (> 2 GHz) but are virtually dispersionless at higher frequencies; and home-built planar bowtie antennas (~ 3 –10 GHz) [12] which are predicted to be minimally dispersive. We may then tailor the dispersion of our link by pairing different antenna geometries; for example, a link employing bowties as both the transmitter

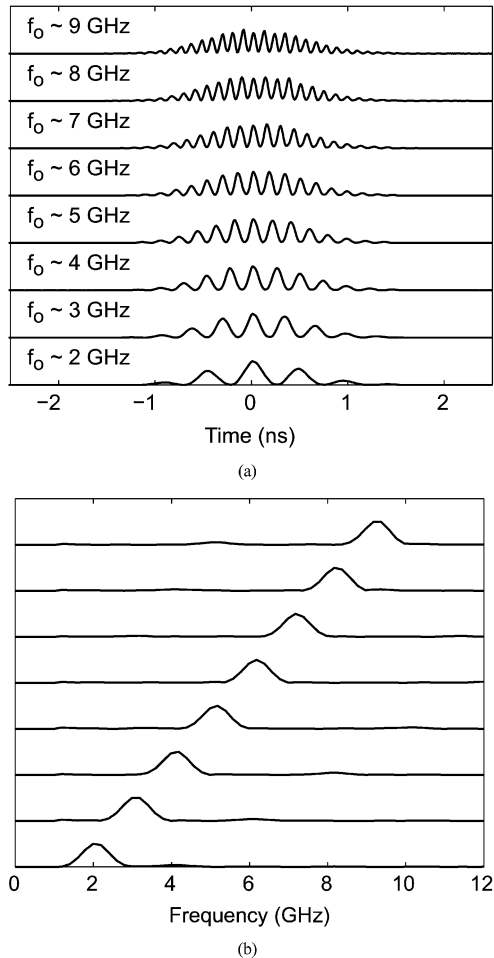


Fig. 2. (a) Fixed-bandwidth, variable center frequency waveforms used to excite the bowtie antenna link. Here, the waveform duration is fixed at ~ 1.14 ns full-width at half maximum (FWHM) to yield a FWHM spectral width of approximately 775 MHz at center frequencies ranging from 2–9 GHz. (b) Calculated power spectral density (FFT) of the excitation waveforms shown in (a). Here, the signal bandwidth remains fixed at ~ 775 MHz as the center frequency is varied from 2–9 GHz.

and receiver is predicted to exhibit minimal waveform dispersion whereas a link consisting of two Archimedean spirals is expected to show strong dispersion.

A. Low-Dispersion Link

To illustrate our technique we first analyze a link predicted to be minimally dispersive; this link consists of a pair of bowtie antennas separated by approximately 1 meter. Note the 1-meter separation satisfies the Rayleigh far-field condition of $R \gg 2d^2/\lambda$ over the majority of the frequency band of 1–10 GHz for the horn antennas. For the Archimedean spiral antennas employed in later measurements, this condition is strongly satisfied over the entire frequency band of interest. We excite our transmitting antenna with a series of 1.14-ns FWHM duration Gaussian impulses amplitude modulated at frequencies ranging from 2–9 GHz as shown in Fig. 2(a). The peak amplitude for our transmit waveforms is approximately 120 mV. To illustrate the frequency content of the excitation waveforms, we show the calculated power spectral densities (FFT) of the measured time-

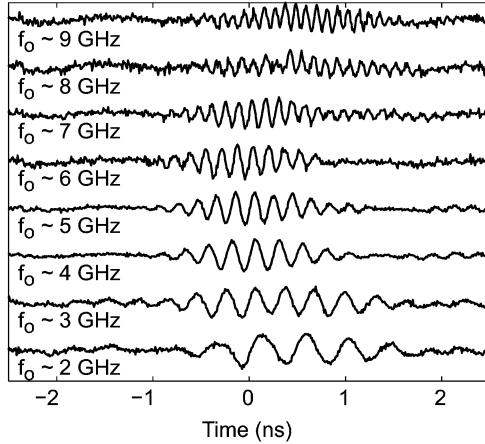


Fig. 3. Received voltage waveforms at the link output for f_o from 2–9 GHz. The waveforms all arrive at the receiver with virtually the same relative delay and show roughly the same duration. The slight broadening and delay (a few hundred picoseconds) observed for center frequencies of 8 and 9 GHz is discussed later in the text. These results illustrate (qualitatively) that the bowtie antenna is minimally dispersive.

domain waveforms of Fig. 2(a) in Fig. 2(b). Here, the signal bandwidth is fixed at ~ 775 MHz as the center frequency is varied from 2–9 GHz. We then measure the arrival time for each waveform at the receiver; the received waveforms (peak voltage ~ 20 mV) are illustrated in Fig. 3. By visually judging the centroid (center-of-mass) of the received waveforms relative to those of the transmitted signals in Fig. 2(a), all arrive at virtually the same delay ($t = 0$ ns) as predicted. There is a slight deviation in arrival time at higher frequencies; however, this deviation is difficult to determine from the measured voltage waveforms given the received signal amplitudes and signal distortion resulting from the frequency response of the bowtie antennas. This difficulty motivates a different visualization and waveform analysis methodology.

To more clearly visualize the dispersion of our antennas, as well as to improve the fidelity of the received waveform data for calculation purposes, we numerically calculate the spectrogram of each received voltage waveform. The spectrogram is a time-frequency technique for characterizing the time-varying nature of a signal's frequency content [13]. Mathematically, the signal of interest $s(t)$ (here, the measured received waveform) is multiplied by a gate function $g(t)$ with a user-defined delay τ . Then, the spectrogram is calculated by Fourier transforming the resulting gated signal to obtain the power spectral density of the signal spectrum as a function of the delay τ

$$S(\tau, \omega) = \left| \int_{-\infty}^{\infty} dt s(t)g(t - \tau)\exp(-j\omega t) \right|^2. \quad (4)$$

For the spectrograms presented in this work, we utilize a ~ 2.1 ns FWHM Gaussian gate function. The spectrograms for each individual received pulse (at each center frequency) are then overlaid to give an intuitive picture of the link dispersion across the 2–9 GHz frequency range. The family of spectrograms for our bowtie antenna link is shown in Fig. 4. Here, each set of concentric rings (a contour plot) is the spectrogram for one pulse cen-

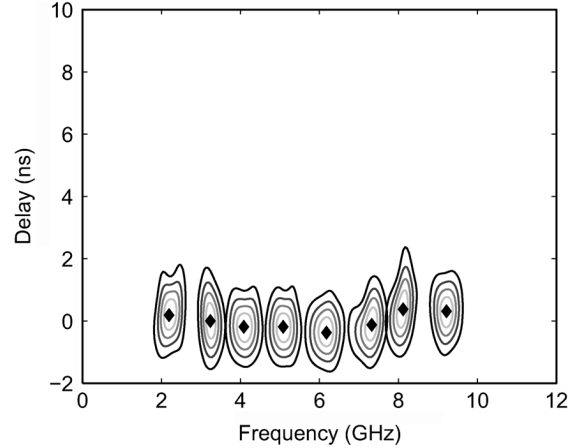


Fig. 4. Spectrograms calculated from each of the measured received waveforms of Fig. 3 using a 2.1 ns FWHM gate function; each set of concentric rings corresponds to the spectrogram of an individual received waveform. Over the range of 2–9 GHz, the received waveforms are seen to arrive at virtually the same instant in time. The black diamonds mark the spectrogram (delay) centroids which vary on ± 375 ps about $t = 0$ ns over the 2–9 GHz frequency range.

tered at a center frequency of f_o that arrives at the receiver with a delay τ —the black diamonds mark the spectrogram maxima.

Several key dispersion characteristics of the antennas/antenna link may be deduced from the data of Fig. 4. First, by comparing the spectrogram maxima, it is clear there is minimal frequency-dependent delay over the 2–9 GHz range; the maximum delay variation is ± 375 ps. Second, by comparing the spread along the delay axis relative to that along the frequency axis, one observes that the delay spread for a given bandwidth remains relatively constant over the frequency range of interest; this is a visual representation of the time-bandwidth product and again reinforces that the bowtie antennas exhibit minimal dispersion over the bandwidth of ~ 2 –10 GHz. We may also use the spectrogram to quantitatively describe the dispersion of our antennas by calculating the time-bandwidth product of the marginal delay and frequency distributions of the spectrogram. The marginal delay and frequency distributions are defined as

$$P_\tau(\tau) = \int d\omega S(\tau, \omega) \quad (5)$$

$$P_\omega(\omega) = \int d\tau S(\tau, \omega). \quad (6)$$

The width of the delay marginal is determined by the duration of the intensity of the cross-correlation of the received waveform $s(t)$ and the gate pulse $g(t)$; the bandwidth of the frequency marginal is determined by the intensity of the cross-correlation of the complex spectra of the received waveform and the gate pulse. As with any signal, the time-bandwidth product of the marginals is minimum when the signal and gate pulses are both unchirped. Here we utilize a bandwidth limited gate pulse; therefore, the minimum time-bandwidth product is achieved for an unchirped received waveform. The Gaussian envelope duration of the transmitted signal (~ 1.14 ns, FWHM) and Gaussian gate function duration (~ 2.1 ns, FWHM) yield a theoretical time-bandwidth product (for the marginal distributions) of $\Delta t \Delta f \approx 1.0$; as a note, this does not account for any

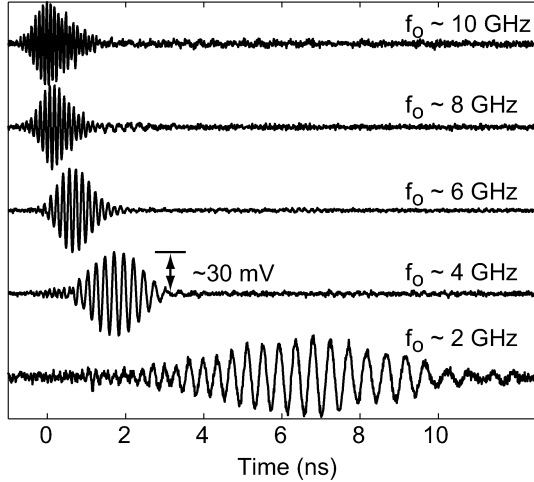


Fig. 5. Received voltage waveforms at the spiral-antenna link output. In contrast to the bowtie antenna link, the spiral link shows clear signs of dispersion; the variation in arrival times is approximately 6.5 ns (almost $6 \times$ the 1.14 ns duration of the excitation waveforms) and there is significant pulse broadening at lower frequencies (the 2 GHz waveform is approximately two-times longer in duration than the 11 GHz waveform of equivalent bandwidth).

frequency-dependent loss in the link (e.g., the $1/f^2$ diffraction loss). Over the range of frequencies between 2–9 GHz, the marginal time-bandwidth product of the received signals in the bowtie link varies from 0.96–1.27. These values show good agreement with the theoretical value predicted for a dispersionless link.

B. Highly-Dispersive Link

Next, we consider a highly-dispersive link consisting of two Archimedean spiral antennas. Given the geometry of the Archimedean spiral antenna, different frequencies radiate at different physical locations on the antenna (specifically, at different radial locations) [11]. This means that the waveform radiated from (or received by) such an antenna will exhibit a strong down-chirp (since the antenna is fed at the center) and the waveform duration will be determined by the overall length of the spiral arms. Here, we again excite the transmitting antenna with a series of ~ 1.14 ns FWHM amplitude-modulated Gaussian waveforms. Given the increased bandwidth of our spiral antennas (as compared to the bowties) we perform our measurements for center frequencies in the range from ~ 2 –11 GHz. For reference, Fig. 2(a) shows our excitation waveforms for center frequencies of $f_0 = 2 - 9$ GHz. The frequency-dependent delay of this antenna link is quite clear upon observation of the received signals, shown in Fig. 5. Here, not only is there a global variation in delay as illustrated by the ~ 6.5 ns difference in arrival time between the $f_0 = 10$ GHz and $f_0 = 2$ GHz signals, but also a strong “local” variation in the delay as exhibited by broadening of the pulse envelope as the center frequency decreases.

The collection of spectrograms for the received waveforms calculated with the same 2.1 ns FWHM Gaussian gate function are shown in Fig. 6. As expected, the strong delay variation is quite apparent here—over the ~ 2 –11 GHz range, the delay varies by approximately 6.5 ns (as determined by the spectrogram maxima shown by the black diamonds). The pulse

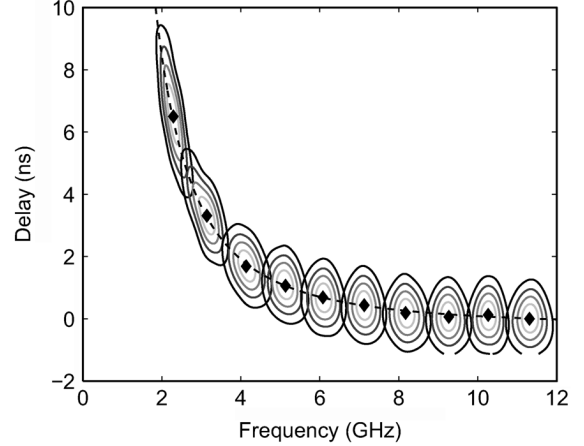


Fig. 6. Spectrograms calculated from the direct delay measurements of the Archimedean spiral antenna link (a subset of the received waveforms is shown in Fig. 5). As expected there is a strong frequency-dependent delay—over the range of 2–11 GHz, the spectrogram maxima (black diamonds) vary by approximately 6.5 ns. The dashed curve shows a numerical fit to the spectrogram maxima obtained from the spiral geometry [see (7)].

broadening at lower frequencies is also quite evident—visually, the marginal time-bandwidth product varies by roughly a factor of $2 \times$ from 2–11 GHz. Numerically, the time-bandwidth product of the marginal distributions varies over the range of ~ 1.2 (11 GHz) $> \Delta t \Delta f > \sim 2.2$ (2 GHz). It is also interesting to note that our spectrogram measurements (in particular the spectrogram maxima) show excellent agreement with the frequency-dependent delay predicted by the Archimedean spiral geometry. It can be shown the frequency-dependent delay contributed by one Archimedean spiral antenna is accurately described by [11]

$$\tau(f) = \frac{u}{2a} \left(\frac{1}{4\pi^2 f^2} - \frac{r_{\min}^2}{u^2} \right). \quad (7)$$

In this expression, r_{\min} (μ m) is the arm radius at the feedpoint, u (cm/ns) is the current velocity along the spiral, and a (μ m/rad) is the spiral growth rate. Using twice the delay predicted by this model (since the receiving antenna contributes an equal delay to that of the transmitting antenna), we perform a numerical fit to the spectrogram maxima shown in Fig. 6. For fit parameters of $r_{\min} \approx 643 \mu$ m, $a \approx 58 \mu$ m/rad, and $u \approx 8$ cm/ns, the delay model matches extremely well with the measured frequency-dependent delay as shown by the dashed curve. For comparison the physically measured feedpoint radius and growth-rate are $r_{\min} \approx 620 \mu$ m and $a \approx 63 \mu$ m/rad which also show excellent agreement with the values determined experimentally from the spectrogram data.

It is interesting to note that locally (i.e., within one spectrogram of the collection), the slope of the frequency-dependent delay may be visualized by the inclination of a single spectrogram, though the nonlinearity of the delay curve is not manifested within a single spectrogram. This is due to the fact that the numeric gate function duration is on the same order as that of a single received waveform, that is, the temporal resolution within a single received signal is limited. Over the entire collection of spectrograms (globally) the temporal resolution is significantly better which leads to the excellent agreement between the delay predicted by (7) and the spectrogram maxima.

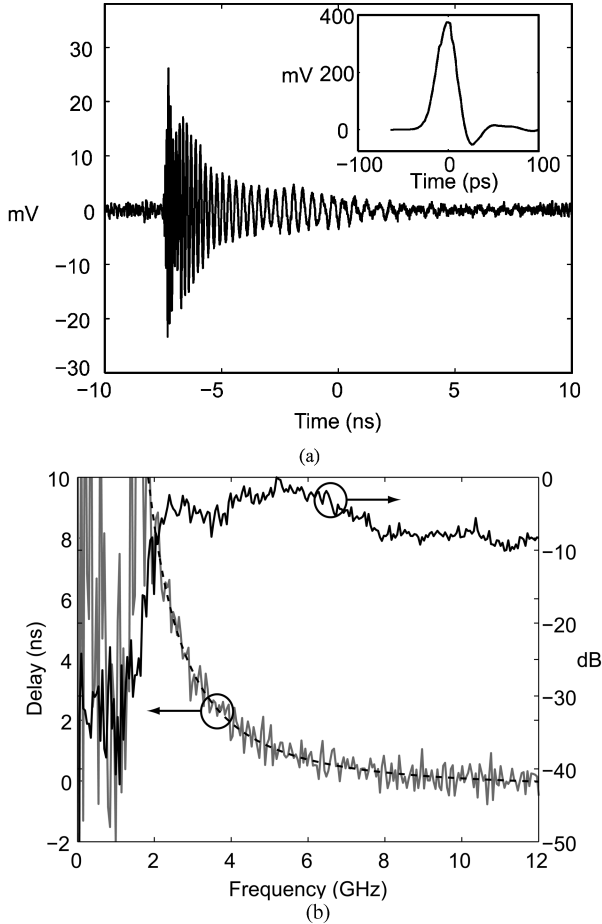


Fig. 7. (a) Impulse response of the Archimedean spiral antenna link; the driving impulse is inset. As predicted from our frequency-dependent delay measurements, the impulse response shows a very strong down-chirp. Here, the impulse response duration extends over 8 ns ($\sim 400 \times$ the impulse duration of 20 ps). (b) Frequency response of the Archimedean spiral antenna link (FFT of the time-domain data). Here, the solid black curve shows the (normalized) power spectral density and the gray curve shows the frequency-dependent delay calculated from the spectral phase via (2). The dashed curve is the same numerical fit previously shown in Fig. 6; the RMS delay error over the range of 2–12 GHz is $\tau_{\text{err}} = 0.4$ ns, which illustrates excellent agreement between direct measurements of the frequency-dependent delay and that obtained via the impulse response.

C. Comparison With Antenna Link Impulse Measurements

As the impulse response is a more commonly-utilized tool for determining the spectral response of a given system (antenna link) in the time-domain, it is useful to compare the frequency-dependent delay acquired through direct measurement with that obtained from the impulse response. For the sake of comparison, we begin by analyzing the Archimedean spiral antenna link. To measure the link impulse response, we excite the transmitting antenna with a ~ 400 mV peak amplitude, ~ 20 ps impulse synthesized by driving the photodiode in our system with an optical pulse directly from our source laser. The measured link impulse response (and driving impulse, inset) are illustrated in Fig. 7(a). As expected from direct measurements of the frequency-dependent delay, the link impulse response shows a strong down-chirp and the waveform extends over ~ 8 ns ($\sim 400 \times$ the excitation impulse duration). While the primary comparisons between these measurements occur in the frequency-domain, there is a key point contained in the time-domain data—the amplitude of

the link impulse response. Here, the excitation impulse shows a peak voltage of ~ 400 mV [approximately $3 \times$ the peak amplitude of the excitation waveforms discussed in the preceding Section IV.A.] The impulse response (received signal), however, shows roughly the same peak voltage (~ 25 mV). The amplitude of the impulse response decays quite rapidly from its peak value whereas in our frequency-dependent delay measurements, the amplitude of the received waveform spends a longer time near its peak amplitude (see Fig. 5). As described in Section II, the amplitude of waveforms from our electromagnetic pulse shaper are subject to a peak-power constraint determined by the input optical energy per pulse and the output waveform duration (length of the fiber stretcher). Subject to this constraint, narrowband excitation waveforms which spend a longer time near the peak-power limit result in more energy in the received signal—this is clearly seen by comparing the amplitudes of the received waveforms of Figs. 5 and 7(a). Therefore, measurement of the frequency-dependent delay (as opposed to the impulse response) provides a higher dynamic range measurement of the link response.

To compare the frequency-dependent delay extracted via direct measurements to that obtained from the impulse response, we take the FFT of the time-domain impulse response to obtain the link frequency response shown in Fig. 7(b). Here, the solid black curve shows the (normalized) power spectral density and the gray curve shows the frequency-dependent delay [derivative of the spectral phase as given by (2)]. The dashed curve is the numeric fit to the spectrogram maxima in Fig. 5 using the delay model of (7). Over the range of 2–12 GHz, the RMS delay error is $\tau_{\text{err}} \approx 0.4$ ns. As is evident, there is excellent agreement between the two measurements illustrating that direct measurements of the frequency-dependent delay provide identical information to that obtained via the impulse response. We may now use the delay information obtained in our measurements to predict the behavior of links constructed from different (dispersive) antennas and to verify aspects of reciprocity; we discuss these aspects of our experiment in the following section.

D. Behavior of Asymmetric Links and Reciprocity

In the preceding experiments, our antenna links were symmetric, i.e., the transmitting and receiving antennas were identical. For such a link then, we are able to extract the spectral phase (frequency-dependent delay) contribution of one antenna through reciprocity [14]—that is, each antenna contributes one half of the total frequency-dependent delay. With the knowledge of this contribution for a collection of antennas, we may then predict the behavior of an asymmetric link (one consisting of different transmitting and receiving antennas).

To illustrate this, we consider a link consisting of an Archimedean spiral antenna and a broadband ridged-horn antenna. In order to describe the behavior of this link, we first characterize the phase-response of the ridged horn by measuring the impulse response of a symmetric ridged horn link. The link impulse response [excitation impulse shown in the inset of Fig. 7(a)] is given in Fig. 8(a). From this response, it is clear that the ridged horn shows minimal dispersion except at the lowest frequencies—the leading portion of the waveform is roughly the derivative of the driving impulse. The low-frequency tail of the waveform extending for several ns is due to strong phase variations near cutoff in the antenna [15].

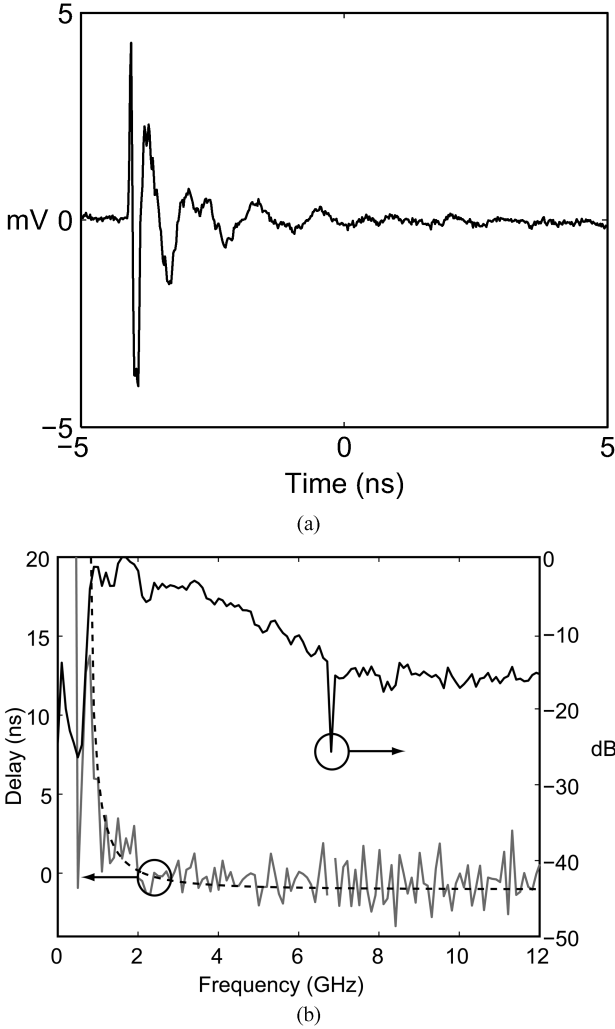


Fig. 8. (a) Impulse response of the symmetric ridged-horn antenna link. (b) Frequency response of the ridged-horn antenna link calculated from the experimental impulse response. The black curve illustrates the (normalized) power spectral density and the gray curve the frequency-dependent delay. As evidenced by both the impulse response in (a) and the frequency-dependent delay in (b), the ridged-horn antenna exhibits minimal dispersion for frequencies above ~ 2 GHz. The dashed curve shows a numerical fit to the data based on a physical model for the ridged-horn antenna [that of a nonuniform transmission line, see (8)].

This strong spectral phase variation is quite evident in the frequency response of the link [shown in Fig. 8(b)]. The solid black curve shows the magnitude of the frequency response; the gray curve shows the frequency-dependent delay. As expected, the delay is quite minimal above ~ 2 GHz, though there is significant variation between ~ 800 MHz and 2 GHz (near cutoff). This delay is well described by treating the ridged horn as a nonuniform transmission [16] line with an adiabatic exponential impedance taper. By deriving the phase constant for this transmission line (of length L) then differentiating to obtain the frequency-dependent delay, we determine the delay for one antenna to be

$$\tau_{\text{RH}}(f) = \frac{L}{u} \left[1 - \left(\frac{f_c}{f} \right)^2 \right]^{-1/2}. \quad (8)$$

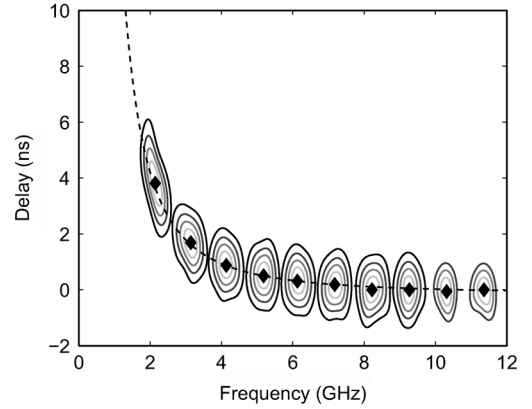


Fig. 9. Spectrograms calculated from direct delay measurements of the asymmetric Archimedean spiral—ridged-horn antenna link (time-domain waveforms are not shown). The delay predicted by the antenna models—the sum of (7) and (8)—agrees with the experimental data quite well. The RMS error between the delay model and spectrogram centroids is ~ 54 ps over the range of 2–11 GHz.

Here, the line length $L = 17.5$ cm (the physical length of the ridged horn antenna), u is the phase velocity along the line, and f_c is the cutoff frequency. Using this model (and multiplying by two to account for both antennas), a numeric fit is performed to the frequency-dependent delay of the ridged horn link. For a phase velocity of $u \approx 15$ cm/ns and a cutoff frequency of $f_c \approx 780$ MHz, the nonuniform transmission line model [dashed line in Fig. 8(b)] shows excellent agreement with the measured frequency-dependent delay in the symmetric ridged-horn link.

With knowledge of the frequency-dependent delay (spectral phase) properties of both the Archimedean spiral and ridged-horn antennas, we may now predict the behavior of the asymmetric link consisting of an Archimedean spiral transmitting antenna and ridged-horn receiving antenna. Mathematically, the frequency-dependent delay should be described by the sum of the contributions from each antenna—the sum of (7) and (8). To observe the frequency-dependent delay of this asymmetric link, we again perform direct measurements of the frequency-dependent delay as detailed previously. For these measurements we utilize the same excitation waveforms as for the symmetric Archimedean spiral link—1.14 ns FWHM Gaussian envelopes amplitude modulated at center frequencies ranging from 2–11 GHz (see Fig. 2(a) for several representative examples). We then calculate the spectrogram for each received signal and display the collection to visualize the delay behavior of the link; the results of these measurements are shown in Fig. 9. The delay variation predicted by evaluating the sum of (7) and (8) (with the same fit parameters determined from the symmetric links) is found to agree with the measured delay variation quite well—the root-mean-square (RMS) error between the spectrogram maxima and the theoretical model is $\tau_{\text{err}} \approx 54$ ps over the range of 2–12 GHz. This yields an estimate (~ 54 ps) for the error bars in our direct delay measurement.

We again may compare the delay information obtained via direct measurement with that extracted from the link impulse response. In addition, we may verify the reciprocal behavior of the link by interchanging the transmit and receive antennas. To accomplish this comparison, the link frequency response is derived via a FFT of the time-domain impulse response (not

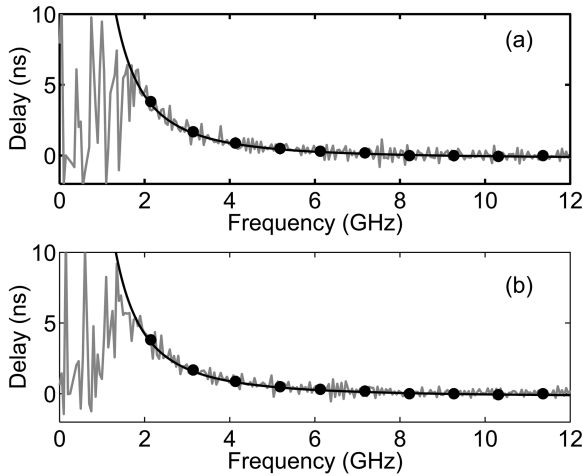


Fig. 10. Frequency-dependent delay for the asymmetric antenna link. (a) Spiral transmitting, ridged-horn receiving. (b) Frequency-dependent delay with the transmitting and receiving antennas reversed. The solid black curves here are the predicted delay calculated from the models for our antenna (previously illustrated in Fig. 9) and the black circles are the spectrogram maxima, also from Fig. 9. Again, the measurements obtained via direct measurements of the delay agree very well with that obtained from the impulse response; over the range of 2–12 GHz in both responses, the RMS delay error is ~ 0.3 ns.

shown). To illustrate reciprocity, impulse response measurements are taken using the Archimedean spiral as the transmitting antenna and the ridged-horn as the receiving antenna; the transmitting and receiving functionality are then reversed and another impulse response is taken. The frequency-dependent delay derived from these measurements is shown in Fig. 10. In Fig. 10(a), the spiral functions as the transmitting antenna and the ridged-horn as the receiving antenna; Fig. 10(b) illustrates the frequency-dependent delay for the link with the transmitting and receiving antennas reversed. Here, there is almost perfect congruity between the frequency-dependent delay derived via time-domain impulse response measurements and that extracted from the link directly. To illustrate this, the spectrogram maxima and numerical fit based on geometric models for the antenna from Fig. 9 are superposed with the delay extracted from the impulse responses. Note, there is excellent agreement between direct measurements of the frequency-dependent delay (only performed using the spiral as the transmitting antenna and the ridged-horn as the receiving antenna), the impulse response, and the theoretical model for the link delay. For both links, the RMS error between the measured frequency-dependent delay (from the impulse response) and the theoretical model is $\tau_{\text{err}} \approx 0.3$ ns—on the order of the fluctuations in the impulse response measurements themselves. Upon comparison of the frequency-dependent delay for the asymmetric link with that for the symmetric Archimedean spiral link [Fig. 7(b)], it is interesting to note the asymmetric link exhibits roughly half the total delay of the symmetric link. This is expected since the asymmetric link shows approximately half the dispersion of the link employing two spiral antennas (i.e., the ridged-horn antenna is minimally dispersive except at very low frequencies).

V. SUMMARY

In this work we present a technique for direct measurement of the frequency-dependent delay (dispersion) behavior of broad-

band antenna structures. This technique is rooted in approaches to dispersion measurement used in the field of high-speed optics and provides correspondent delay information to that obtained via impulse response measurements. The use of spectrograms to view and analyze our direct delay measurements is also shown to provide an intuitive view of the effects of a particular antenna geometry on broadband excitation waveforms. With excellent sensitivity—RMS errors as low as ~ 54 ps for delay variations on the order of 10 ns—this technique provides a suitable alternative to time-domain impulse response measurements geared to extract the dispersion properties of broadband antennas. We emphasize our technique provides equivalent information to—and complements—swept-frequency measurements (those taken with a network analyzer); our apparatus and technique are particularly relevant to those performing research in impulsive UWB systems (i.e., with some time-domain measurement capabilities, such as a fast oscilloscope) in that exact same electromagnetic pulse shaping apparatus may be utilized to both measure and compensate for these distortions in such systems.

ACKNOWLEDGMENT

This work was performed at Purdue University, West Lafayette, IN. The authors would like to thank X. Liu for fabricating the planar bowtie antennas.

REFERENCES

- [1] J. S. Lee, C. Nguyen, and T. Scullion, "A novel, compact, low-cost, impulse ground-penetrating radar for nondestructive evaluation of pavements," *IEEE Trans. Instrum. Meas.*, vol. 53, pp. 1502–1509, 2004.
- [2] M. Z. Win and R. A. Scholtz, "Ultra-wide bandwidth time-hopping spread-spectrum impulse radio for wireless multiple-access communications," *IEEE Trans. Commun.*, vol. 48, pp. 679–691, 2000.
- [3] M. Farhang and J. A. Salehi, "Spread-time/time-hopping UWB cdma communication," in *Proc. IEEE Int. Symp. on Communications and Information Technologies (ISCIT 2004)*, 2004, pp. 1047–1050.
- [4] "Understanding the fundamental principles of vector network analysis," Agilent Technologies Application Note, AN 1287-1 2000.
- [5] W. H. Knox, N. M. Pearson, K. D. Li, and C. A. Hirlimann, "Interferometric measurements of femtosecond group delay in optical components," *Opt. Lett.*, vol. 13, pp. 574–576, 1988.
- [6] I. Lin, J. D. McKinney, and A. M. Weiner, "Photonic synthesis of broadband microwave arbitrary waveforms applicable to UWB communication," *IEEE Microw. Wireless Compon. Lett.*, vol. 15, pp. 226–228, 2005.
- [7] J. D. McKinney, I. S. Lin, and A. M. Weiner, "Shaping the power spectrum of UWB radio-frequency signals," *IEEE Trans. Microw. Theory Tech.*, vol. 54, no. 12, pp. 4247–4255, 2006.
- [8] J. Chou, Y. Han, and B. Jalali, "Adaptive RF-photonics arbitrary waveform generator," *IEEE Photon. Technol. Lett.*, vol. 15, pp. 581–583, 2003.
- [9] J. H. Reed, Ed., *An Introduction to Ultra Wideband Communication Systems*. Englewood Cliffs, NJ: Prentice Hall, 2005.
- [10] T. W. Hertel and G. S. Smith, "On the dispersive properties of the conical spiral antenna and its use for pulsed radiation," *IEEE Trans. Antennas Propag.*, vol. 51, pp. 1426–1433, 2003.
- [11] J. A. Kaiser, "The Archimedean two-wire spiral antenna," *IRE Trans. Antennas Propag.*, pp. 312–323, 1960.
- [12] K. Kiminami, A. Hirata, and T. Shiozawa, "Double-sided printed bow-tie antenna for UWB communications," *IEEE Antennas Wireless Propag. Lett.*, vol. 3, pp. 152–153, 2004.
- [13] L. Cohen, "Time-frequency distributions—a review," *Proc. IEEE*, vol. 77, pp. 941–981, 1989.
- [14] G. S. Smith, "A direct derivation of a single-antenna reciprocity relation for the time domain," *IEEE Trans. Antennas Propag.*, vol. 52, pp. 1568–1577, 2004.
- [15] J. D. McKinney and A. M. Weiner, "Compensation of the effects of antenna dispersion on UWB waveforms via optical pulse shaping techniques," *IEEE Trans. Microw. Theory Tech.*, vol. 54, no. 4, pp. 1681–1686, 2006.
- [16] S. Ramo, J. R. Whinnery, and T. Van Duzer, *Fields and Waves in Communication Electronics*, 3rd ed. New York: Wiley, 1994.



Jason D. McKinney (S'99–M'03) received the Ph.D. degree in electrical engineering from Purdue University, West Lafayette, IN, in 2003.

From July 2001 through May 2003, he was a Graduate Assistance in Areas of National Need (GAANN) Fellow; as such he was active in both teaching and research at Purdue. His doctoral work included the first demonstration of ultrafast optical pulse shaping techniques for synthesis of arbitrarily shaped millimeter waveforms exhibiting arbitrary phase and frequency modulation at center frequencies up to 50 GHz. After

completing his Ph.D., he was a Visiting Assistant Professor, from 2003 to 2005, and a Research Scientist, from 2005 to 2006, in the School of Electrical and Computer Engineering at Purdue University. He is currently with the Microwave Photonics Section, Optical Sciences Division, U.S. Naval Research Laboratory. His research interests include low-noise, high-power analog optical links, ultrafast optical pulse processing and applications of photonics in ultrabroadband microwave systems. He has authored or coauthored over 14 journal articles, one book chapter, and over 27 conference papers.

Dr. McKinney is a member of both the Optical Society of America (OSA). He has received a variety of awards for his research, most notably, the Chorafas Prize for doctoral research in 2003 (awarded to one Purdue doctoral student per year) and as a finalist for the Optical Society of America/New Focus Student Award in 2002. He has also received numerous awards in recognition of his teaching and is an Associate Fellow of the Purdue University Teaching Academy.



Dimitrios Peroulis (S'99–M'04) received the Diploma degree in electrical and computer engineering from the National Technical University of Athens, Athens, Greece, in 1998, and the M.S.E. and Ph.D. degrees in electrical engineering from The University of Michigan, Ann Arbor, in 1999 and 2003, respectively.

Since August 2003, he has been an Assistant Professor at the School of Electrical and Computer Engineering, Purdue University, West Lafayette, IN. His current research work is focused on microelectromechanical systems (MEMS) for multifunctional communications systems and sensors.

Dr. Peroulis has received several teaching awards from Purdue University including the Teaching for Tomorrow Award in 2006. He has also been the recipient of three Student Paper Awards at IEEE MTT-S in 2001 and 2002 and the IEEE AP-S in 2001.



Andrew M. Weiner (F'95) received the Sc.D. degree in electrical engineering from the Massachusetts Institute of Technology (MIT), Cambridge, in 1984.

Upon graduation he joined Bellcore, first as Member of Technical Staff and later as Manager of Ultrafast Optics and Optical Signal Processing Research. He moved to Purdue University, West Lafayette, IN, in 1992 and is currently the Scifres Distinguished Professor of Electrical and Computer Engineering. His research focuses on ultrafast optics signal processing and applications to high-speed

optical communications and ultrawideband wireless. He is especially well known for his pioneering work in the field of femtosecond pulse shaping, which enables generation of nearly arbitrary ultrafast optical waveforms according to user specification. He has been author or coauthor of over 300 conference papers, including approximately 80 conference invited talks, and has presented over 70 additional invited seminars at university, industry, and government organizations. He has published six book chapters and over 190 journal articles. He holds nine U.S. patents.

Prof. Weiner is a Fellow of the Optical Society of America and has won numerous awards for his research. He has served as Co-Chair of the Conference on Lasers and Electro-optics and the International Conference on Ultrafast Phenomena and as Associate Editor of several journals. He has also served as Secretary/Treasurer of IEEE LEOS and as a Vice-President of the International Commission on Optics (ICO).